


## Edge-and strain-induced band bending in bilayer-monolayer $Pb_2Se_3$ heterostructures

Peng Fan(范朋), Guojian Qian(钱国健), Dongfei Wang(王东飞), En Li(李恩), Qin Wang(汪琴), Hui Chen(陈辉), Xiao Lin(林晓), and Hong-Jun Gao(高鸿钧)

**Citation:**Chin. Phys. B, 2021, 30 (**1**): 018105. DOI: 10.1088/1674-1056/abcf92
Journal homepage: http://cpb.iphy.ac.cn; http://iopscience.iop.org/cpb

**What follows is a list of articles you may be interested in**

---

## Epitaxial synthesis and electronic properties of monolayer $Pd_2Se_3$

Peng Fan(范朋), Rui-Zi Zhang(张瑞梓), Jing Qi(戚竞), En Li(李恩), Guo-Jian Qian(钱国健), Hui Chen(陈辉), Dong-Fei Wang(王东飞), Qi Zheng(郑琦), Qin Wang(汪琴), Xiao Lin(林晓), Yu-Yang Zhang(张余洋), Shixuan Du(杜世萱), Hofer W A, Hong-Jun Gao(高鸿钧)

Chin. Phys. B, 2020, 29 (**9**): 098102. DOI: 10.1088/1674-1056/abab80

## Epitaxial growth and air-stability of monolayer $Cu_2Te$

K Qian(钱凯), L Gao(高蕾), H Li(李航), S Zhang(张帅), J H Yan(严佳浩), C Liu(刘晨), J O Wang(王嘉鸥), T Qian(钱天), H Ding(丁洪), Y Y Zhang(张余洋), X Lin(林晓), S X Du(杜世萱), H-J Gao(高鸿钧)

Chin. Phys. B, 2020, 29 (**1**): 018104. DOI: 10.1088/1674-1056/ab5781

## Growth of high quality $Sr_2IrO_4$ epitaxial thin films onconductive substrates

Hui Xu(徐珲), Zhangzhang Cui(崔璋璋), Xiaofang Zhai(翟晓芳), Yalin Lu(陆亚林)

Chin. Phys. B, 2019, 28 (**7**): 078102. DOI: 10.1088/1674-1056/28/7/078102

## Two-step growth of $VSe_2$ films and their photoelectric properties

Yu Zeng(曾玉), Shengli Zhang(张生利), Xiuling Li(李秀玲), Jianping Ao(敖建平), Yun Sun(孙云), Wei Liu(刘玮), Fangfang Liu(刘芳芳), Peng Gao(高鹏), Yi Zhang(张毅)

Chin. Phys. B, 2019, 28 (**5**): 058101. DOI: 10.1088/1674-1056/28/5/058101

## Growth of high-quality perovskite (110)-$SrIrO_3$ thin films using reactive molecular beam epitaxy

Kai-Li Zhang(张凯莉), Cong-Cong Fan(樊聪聪), Wan-Ling Liu(刘万领), Yu-Feng Wu(吴宇峰), Xiang-Le Lu(卢祥乐), Zheng-Tai Liu(刘正太), Ji-Shan Liu(刘吉山), Zhong-Hao Liu(刘中灏), Da-Wei Shen(沈大伟)

Chin. Phys. B, 2018, 27 (**8**): 088103. DOI: 10.1088/1674-1056/27/8/088103

---

RAPID COMMUNICATION

# Edge- and strain-induced band bending in bilayer-monolayer $Pb_2Se_3$ heterostructures*

Peng Fan(范朋)[1], Guojian Qian(钱国健)[1], Dongfei Wang(王东飞)[1], En Li(李恩)[1], Qin Wang(汪琴)[1], Hui Chen(陈辉)[1,2], Xiao Lin(林晓)[1,2], and Hong-Jun Gao(高鸿钧)[1,2,†]

[1] *Institute of Physics and University of Chinese Academy of Sciences, Chinese Academy of Sciences, Beijing* 100190, *China*
[2] *CAS Center for Excellence in Topological Quantum Computation, Beijing* 100190, *China*

(Received 4 November 2020; revised manuscript received 20 November 2020; accepted manuscript online 2 December 2020)

By using scanning tunneling microscope/microscopy (STM/STS), we reveal the detailed electronic structures around the sharp edges and strained terraces of lateral monolayer-bilayer $Pd_2Se_3$ heterostructures. We find that the edges of such heterostructures are well-defined zigzag type. Band bending and alignment are observed across the zigzag edge, forming a monolayer-bilayer heterojunction. In addition, an n-type band bending is induced by strain on a confined bilayer $Pd_2Se_3$ terrace. These results provide effective toolsets to tune the band structures in $Pd_2Se_3$-based heterostructures and devices.

**Keywords:** $Pd_2Se_3$, band bending, lateral heterostructures, scanning tunneling microscope/spectroscopy

**PACS:** 81.15.–z, 81.05.Zx, 68.37.Ef, 68.37.Ps **DOI:** 10.1088/1674-1056/abcf92

## 1. Introduction

Transition metal selenides have emerged as important two-dimensional (2D) semiconductor candidates for applications of electronics, optoelectronics, and thermoelectric nanodevices.[1–4] The traditional 2D semiconductors that derived from layered bulk materials such as $WS_2$ and $MoS_2$ have seen a huge advancement in electronics and optoelectronics using all 2D materials.[5–10] Furthermore, layer-dependent band engineering and construction of lateral heterostructures based on 2D materials with different thickness create new possibilities for device applications.[11–14] However, the further development in the field requires the continual investigation of 2D materials systems beyond those that are well known. In addition, creating 2D materials that do not exist as bulk layered materials remains to be fully explored.[15]

Recently, new types of 2D semiconductors without layered bulk counterpart have attracted tremendous attention due to the predicted novel properties beyond the traditional 2D materials.[16–23] Among them, $Pd_2Se_3$ is regarded to be an ideal optoelectronics material as it exhibits anisotropic transport properties, moderate band gap, and excellent absorption in a wide range of the solar spectrum.[24–26] In experiments, it is impossible to obtain monolayer (ML) and few layer $Pd_2Se_3$ through mechanical exfoliation due to the lack of layered bulk materials. So far, ML $Pd_2Se_3$ has been synthesized through phase transformation from bilayer (BL) $PdSe_2$ induced by electron irradiation[27–29] or thermal annealing.[30] However, fabricating BL $Pd_2Se_3$ and studying the thickness dependence electronic properties have not been explored.

Here, we report the construction of BL $Pd_2Se_3$ islands and BL–ML lateral heterostructures on the graphene-SiC(0001) substrate. By using scanning tunneling microscope/spectroscopy (STM/S), we show a sharp and well-defined zigzag edge formed on the interface between BL and ML $Pd_2Se_3$. Band bending and alignment are observed across the interface due to the thickness dependence of the bandgap. In addition, the band bending induced by strain on the deformation can be clearly observed on the confined BL terrace.

## 2. Methods

The sample was synthesized by molecular beam epitaxy in a commercial ultrahigh vacuum (UHV) STM system with a base pressure of $2.0 \times 10^{-10}$ mbar. A nitrogen-doped 6H-SiC(0001) was flashed to 1550 K, leading to a graphene terminated surface. The atomic beams of Pd (99.95%, Alfa Aesar) and Se (99.999%, Alfa Aesar) were simultaneously deposited at a ratio of $\sim 1:10$ by a Knudsen cell (K-cell) evaporator with the substrate maintained at 500 K. Before measurements, the sample was post-annealed at 475 K for 30 min in a Se-sufficient condition. Differential conductance ($\mathrm{d}I/\mathrm{d}V$) spectra were acquired by a standard lock-in amplifier at a frequency of 973.1 Hz with a 20 mVrms modulation. The tip calibration was performed on an Au(111) substrate.

*Project supported by the National Key Research and Development Project of China (Grant Nos. 2016YFA0202300, 2018YFA0305800, and 2019YFA0308500), the National Natural Science Foundation of China (Grant Nos. 61888102 and 52022105), the Strategic Priority Research Program of Chinese Academy of Sciences (Grant Nos. XDB30000000 and XDB28000000), and the University of Chinese Academy of Sciences.

†Corresponding author. E-mail: hjgao@iphy.ac.cn

© 2021 Chinese Physical Society and IOP Publishing Ltd 

## 3. Results and discussion

The $Pd_2Se_3$ is thermally transferred from epitaxial BL $PdSe_2$ film on graphene through post annealing in vacuum[30] (detailed please refer to the method part). The typical large-scale STM image in Fig. 1(a) shows that a BL $Pd_2Se_3$ island is grown on the ML $Pd_2Se_3$. The BL $Pd_2Se_3$ islands are rectangular-shaped with a width of tens of nanometers. A striated $Pd_2Se_3$ structure with a width of around 1 nm is observed stacked on the top of the BL island.[28] From the line profile along the blue arrow shown in Fig. 1(b), we can get that the height of step edge between the top and bottom $Pd_2Se_3$ layers is 7.5 Å (Fig. 1(b)), which is comparable to the value in ML $Pd_2Se_3$/graphene (7.3 Å).

To investigate the interface between two $Pd_2Se_3$ layers, we got a high-resolution STM image across the step edge and display it in Fig. 2(a). Elliptical dimer protrusions that forming a square lattice (blue box in Fig. 2(a)) are observed on both layers. The lattice constants are $a = 5.90$ Å and $b = 6.03$ Å, which are in agreement with the calculated values of $Pd_2Se_3$.[25] There are two groups of Se atoms in the sandwich $Pd_2Se_3$ structure, which are labeled as $Se_A$ and $Se_B$, respectively. The $Se_B$ is slightly lower than $Se_A$. The two neighboring $Se_A$ atoms are bonding together and form Se-Se dimer structure, while the $S_B$ atoms are distributed separately. Therefore, in the STM image, the local density of states of the surface is dominated by $Se_A$ atoms forming dimer patterns, while $Se_B$ atoms are hardly to be observed due to the lower height than $Se_A$ atoms.[30] We superimpose the model of top-layer Se atoms of $Pd_2Se_3$ onto the STM image, showing that the lattice across the BL and ML $Pd_2Se_3$ is continuous. Therefore, we conclude that the top $Pd_2Se_3$ layer is A-A stacked on the bottom layer and the interface between the two layers has a well-defined zigzag type configuration (Figs. 2(b) and 2(c)).

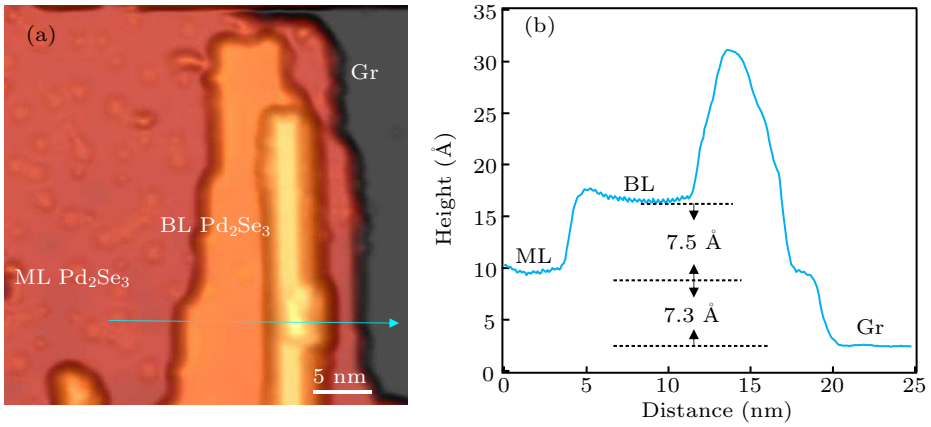



**Fig. 1.** Construction of BL–ML $Pd_2Se_3$ lateral heterostructures. (a) Topographic STM image ($V_S = -1$ V, $I_t = 10$ pA) showing BL–ML $Pd_2Se_3$ lateral heterostructures grown on a graphene/SiC(0001) substrate. (b) Line-profile along the blue arrow in (a), showing the height between two $Pd_2Se_3$ layers.

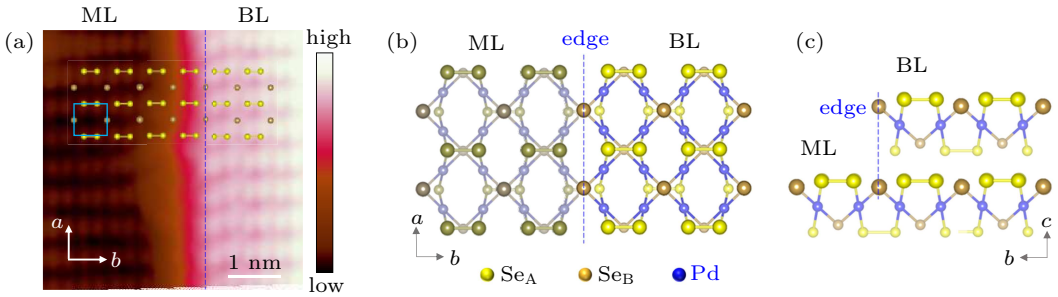



**Fig. 2.** Atomically sharp interface between BL and ML $Pb_2Se_3$. (a) Atomic-resolution STM image ($V_S = -1$ V, $I_t = 10$ pA) of step edge between BL and ML $Pb_2Se_3$. Top view (b) and side view (c) of BL–ML $Pb_2Se_3$ lateral heterostructures with zigzag type interface.

To explore the electronic properties of the sharp interface, we collected series of $dI/dV$ spectra across the BL–ML edge as shown in Fig. 3. Figure 3(a) shows the spatial locations where the $dI/dV$ spectra given in Figs. 3(b) and 3(c) are carried out. The $dI/dV$ spectra are displayed in a logarithmic scale in Figs. 3(b) and 3(c). The numbers on the spectra refer to their positions in the complete set, in which $dI/dV$ spectra are acquired every 0.5 nm from the BL into the ML region, with spectrum #10 acquired at the interface. As the selected $dI/dV$ spectra in Fig. 3(c) show, when the tip is far from the interface, the ML $Pd_2Se_3$ region exhibits a bandgap of about 1.2 eV, while the BL region exhibits a band gap of 1.1 eV. It indicates that $Pd_2Se_3$ exhibits layer dependent bandgap, similar to the results of $PdSe_2$.[31,32]

The intensity plot of $dI/dV$ spectra in Fig. 3(b) and the selected $dI/dV$ spectra in different regions in Fig. 3(c) show the apparent band bending for both conduction band and valence band in the BL region near the interface. The magni-

tude of the band bending is about 0.17 eV over about 4 nm towards the interface. While the spectra in the ML region, in contrast, exhibit little band bending. It is noticed that pronounced band bending is absent in the edge across ML $Pd_2Se_3$ and graphene substrate. These results indicate that the ML and BL bulk bands align to form a type-I heterojunction due to the thickness dependence of the bandgap and band edges.[13]

Except for the zigzag edge, the lattice strain induced band bending is also observed in the confined BL $Pd_2Se_3$ terrace. Figure 4(a) shows a typical confined BL terrace. Several one-dimensional structures are observed on its left side, which are attributed to the striated $Pd_2Se_3$ according to the atomically-resolved STM images, previous scanning transmission electron microscopy images, and calculations based on density functional theory.[28] On the right side, a grain boundary forms on the ML $Pd_2Se_3$, where two different lattice directions highlighted by the red dashed lines and green dashed lines are clearly observed. Therefore, we speculate that the deformation forms on $Pd_2Se_3$ terrace originates from the spatial confinement between the nanoribbons and grain boundary. In order to clarify the structure of the deformation, we display the zoom-in STM image in Fig. 4(b), which is the same area highlighted by the black box in Fig. 4(a). We trace the lattice structure by dashed green curves and find that the lattice structure has a slight in-plain bending.

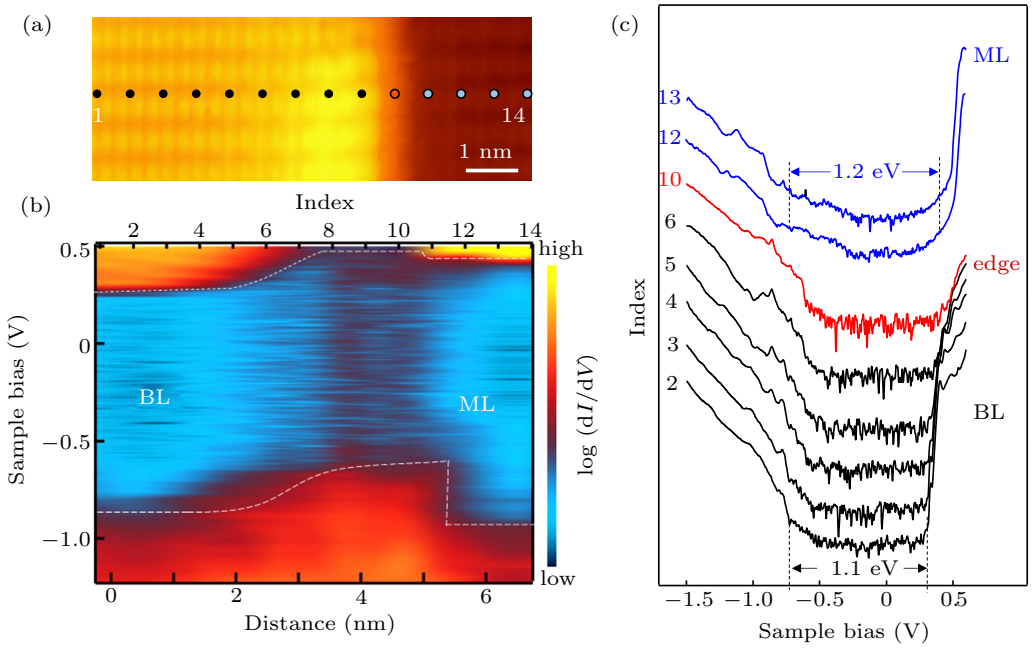



**Fig. 3.** Band profile across the edge of BL–ML $Pb_2Se_3$ lateral heterostructures. (a) STM image ($V_S = -1$ V, $I_t = 10$ pA) of a typical $Pb_2Se_3$ edge. The spectra numbers in (b) and (c) are counted from left to right in the path, while spectrum #10 was taken right at the BL–ML interface. (b) Intensity plot of logarithm of $dI/dV$ spectra, imaging the band profile across the interface. (c) Selected logarithm of $dI/dV$ spectra ($V_S = -1$ V, $I_t = 100$ pA) detected at the colored points in (a), showing the band bending across the interface between BL and ML regions. The edges of valence band, conduct band, and corresponding energy gap in ML and BL regions are highlighted, respectively.

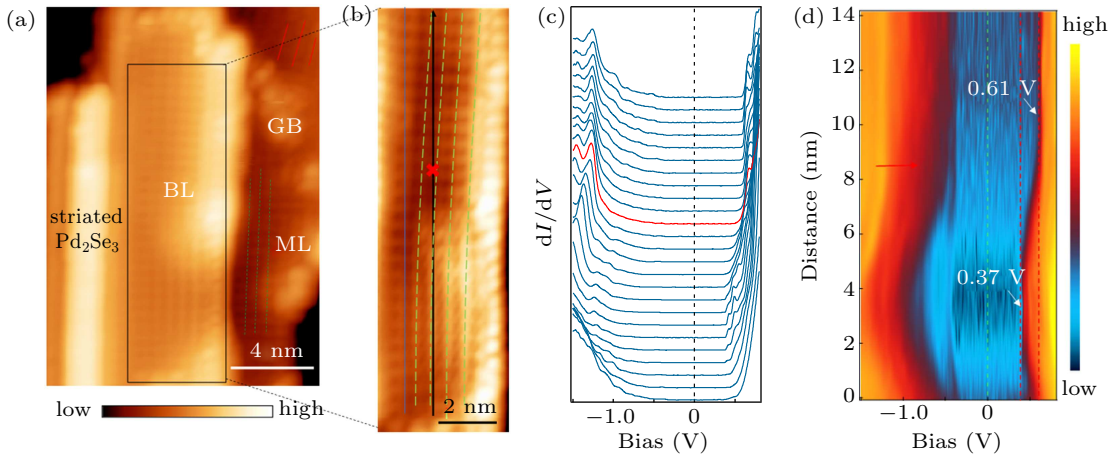



**Fig. 4.** Strain-induced band bending on a confined BL $Pb_2Se_3$ terrace. (a) Topographic STM image ($V_S = -0.8$ V, $I_t = 10$ pA) of BL $Pb_2Se_3$. The dashed red lines and dashed green lines highlight the lattice directions on the ML $Pb_2Se_3$, respectively. (b) Zoom-in STM image ($V_S = -0.8$ V, $I_t = 10$ pA) of the area marked by the black box in (a). The dashed green lines highlight the in-plane bending of the lattice structure. (c) Waterfall-like plot of 25 $dI/dV$ spectra ($V_S = -1$ V, $I_t = 100$ pA) detected along the arrowed black line in (b). The red curve is detected at the position marked by red cross in (b), where the strain is released. (d) Intensity plot of (c). The red arrow marks the position where the strain is released. The energy positions of conduction-band minimum at the bending site and strain-free site are labeled.

To investigate the influence of the strain caused by in-plane bending, we detect 25 $\mathrm{d}I/\mathrm{d}V$ spectra and display them as a waterfall-like plot in Fig. 4(c). The bandgap shifts to the valence band when getting close to the deformation and then shifts back towards the conduct band when getting away from deformation. The red curve is detected at the red cross in Fig. 4(b). The bandgap recovers near this site, indicating that the strain is released. Figure 4(d) is the intensity plot of logarithm of Fig. 4(c). The intensity pointed by the red arrow corresponds to the red curve in Fig. 4(c). We can clearly see a band bending of the deformation, which indicates that the strain induced by in-plane bending of lattice structure has an n-doping effect. It is worthy to notice that the energy gap of one-dimensional strained $Pd_2Se_3$ nanoribbons is smaller than 0.05 eV, which should not contribute to such in-plane band bending in the strained $Pd_2Se_3$.

## 4. Conclusion

We have successfully synthesized BL $Pd_2Se_3$ on graphene-SiC(1000). Our results show the effects of edge and strain on the electronic properties of $Pd_2Se_3$. The band of BL $Pd_2Se_3$ is bending at the ML–BL interface, which forms a heterojunction. For the strain induced by in-plane bending of lattice structure, a n-doped band bending can be clearly observed. Our finding provides several effective ways to develop practical nanodevices based on $Pd_2Se_3$ heterostructures.

## References


[1] Li G, Zhang Y Y, Guo H, Huang L, Lu H L, Lin X, Wang Y L, Du S X and Gao H J 2018 *Chem. Soc. Rev.* **47** 6073
[2] Allain A, Kang J H, Banerjee K and Kis A 2015 *Nat. Mater.* **14** 1195
[3] Song X F, Hu J L and Zeng H B 2013 *J. Mater. Chem. C* **1** 2952
[4] Wang Q H, Kalantar-Zadeh K, Kis A, Coleman J N and Strano M S 2012 *Nat. Nanotechnol.* **7** 699
[5] Manzeli S, Ovchinnikov D, Pasquier D, Yazyev O V and Kis A 2017 *Nat. Rev. Mater.* **2** 17033
[6] Wang H M, Li C H, Fang P F, Zhang Z L and Zhang J Z 2018 *Chem. Soc. Rev.* **47** 6101
[7] Lu J C, Bao D L, Qian K, Zhang S, Chen H, Lin X, Du S X and Gao H J 2017 *ACS Nano* **11** 1689
[8] Chen H, Keiser C, Du S X, Gao H J, Sutter P and Sutter E 2017 *Phys. Chem. Chem. Phys.* **19** 32473
[9] Wang A, Liu Z, Pan J, Li Q, Li G, Huan Q, Du S and Gao H J 2020 *Chin. Phys. B* **29** 078102
[10] Zhang S, Song Y, Li H, Li J M, Qian K, Liu C, Wang J O, Qian T, Zhang Y Y, Lu J C, Ding H, Lin X, Pan J B, Du S X and Gao H J 2020 *Chin. Phys. Lett.* **37** 068103
[11] Zhang J F, Xie W Y, Zhao J J and Zhang S B 2017 *D Mater.* **4** 015038
[12] Guo Y Z and Robertson J 2016 *Appl. Phys. Lett.* **108** 233104
[13] Zhang C D, Chen Y X, Huang J K, Wu X X, Li L J, Yao W, Tersoff J and Shih C K 2016 *Nat. Commun.* **7** 10349
[14] Ou Y, Kang Z, Liao Q L, Zhang Z and Zhang Y 2020 *Nano Res.* **13** 701
[15] Wang F, Wang Z X, Shifa T A, Wen Y, Wang F M, Zhan X Y, Wang Q S, Xu K, Huang Y, Yin L, Jiang C and He J 2017 *Adv. Funct. Mater.* **27** 1603254
[16] Al Balushi Z Y, Wang K, Ghosh R K, Vila R A, Eichfeld S M, Caldwell J D, Qin X Y, Lin Y C, DeSario P A, Stone G, Subramanian S, Paul D F, Wallace R M, Datta S, Redwing J M and Robinson J A 2016 *Nat. Mater.* **15** 1166
[17] Bihlmayer G, Sassmannshausen J, Kubetzka A, Blugel S, von Bergmann K and Wiesendanger R 2020 *Phys. Rev. Lett.* **124** 126401
[18] Vogt P, De Padova P, Quaresima C, Avila J, Frantzeskakis E, Asensio M C, Resta A, Ealet B and Le Lay G 2012 *Phys. Rev. Lett.* **108** 155501
[19] Li N N, Zhang Y, Cheng R Q, Wang J J, Li J, Wang Z X, Sendeku M G, Huang W H, Yao Y Y, Wen Y and He J 2019 *ACS Nano* **13** 12662
[20] Qian K, Gao L, Chen X Y, Li H, Zhang S, Zhang X L, Zhu S Y, Yan J H, Bao D L, Cao L, Shi J A, Lu J C, Liu C, Wang J, Qian T, Ding H, Gu L, Zhou W, Zhang Y Y, Lin X, Du S X, Ouyang M, Pantelides S T and Gao H J 2020 *Adv. Mater.* **32** 1908314
[21] Loffler D, Uhlrich J J, Baron M, Yang B, Yu X, Lichtenstein L, Heinke L, Buchner C, Heyde M, Shaikhutdinov S, Freund H J, Wlodarczyk R, Sierka M and Sauer J 2010 *Phys. Rev. Lett.* **105** 146104
[22] Gao L, Sun J T, Lu J C, Li H, Qian K, Zhang S, Zhang Y Y, Qian T, Ding H, Lin X, Du S and Gao H J 2018 *Adv. Mater.* **30** 1707055
[23] Guo H, Wang X Y, Bao D L, Lu H L, Zhang Y Y, Li G, Wang Y L, Du S X and Gao H J 2019 *Chin. Phys. B* **28** 078103
[24] Naghavi S S, He J, Xia Y and Wolverton C 2018 *Chem. Mater.* **30** 5639
[25] Zhu X, Li F, Wang Y, Qiao M and Li Y 2018 *J. Mater. Chem. C* **6** 4494
[26] Xu X T, Robertson J and Li H L 2020 *Phys. Chem. Chem. Phys.* **22** 7365
[27] Chen J, Ryu G H, Sinha S and Warner J H 2019 *ACS Nano* **13** 8256
[28] Ryu G H, Zhu T, Chen J, Sinha S, Shautsova V, Grossman J C and Warner J H 2019 *Adv. Mater.* **31** 1904251
[29] Lin J, Zuluaga S, Yu P, Liu Z, Pantelides S T and Suenaga K 2017 *Phys. Rev. Lett.* **119** 016101
[30] Fan P, Zhang R Z, Qi J, Li E, Qian G J, Chen H, Wang D F, Zheng Q, Wang Q, Lin X, Zhang Y Y, Du S, W A H and Gao H J 2020 *Chin. Phys. B* **29** 098102
[31] Oyedele A D, Yang S Z, Liang L B, Puretzky A A, Wang K, Zheng J J, Yu P, Pudasaini P R, Ghosh A W, Liu Z, Rouleau C M, Sumpter B G, Chisholm M F, Zhou W, Rack P D, Geohegan D B and Xiao K 2017 *J. Am. Chem. Soc.* **139** 14090
[32] Zhang G, Amani M, Chaturvedi A, Tan C L, Bullock J, Song X H, Kim H, Lien D H, Scott M C, Zhang H and Javey A 2019 *Appl. Phys. Lett.* **114** 253102